# Predictive models of Cannabinoid-1 receptor antagonists derived from diverse classes

Nam Sook Kang *, Gil Nam Lee, Sung-Eun Yoo

*Drug Discovery Platform Technology Team, Korea Research Institute of Chemical Technology, PO Box 107, Yuseong-gu, Daejeon 305-600, Republic of Korea*

## ABSTRACT

Chemical database design is an important consideration for screening processes in drug discovery. More specifically, classification of a diverse compound set deeply influences the validation and the predictive power of prediction model for the designing of *novel* compounds. In this work, we investigated the effect of the reasonable classification on the prediction model. We first collected the known Cannabinoid-1 receptor antagonists. Following this, we calculate the chemical descriptors in order to classify the collected compounds. Finally, we build two predictive models via the 3D-QSAR using different molecular alignment and the alignment independent Molecular Interaction Field models.

© 2009 Elsevier Ltd. All rights reserved.

For an identification and refinement of novel compounds, it is very important that one starts from a diverse and non-redundant set of compounds. Maximum dissimilarity and clustering methods for the designing of compound subsets, therefore, were investigated in order to obtain information on efficiency enhancement of the virtual screening.[1–3] Through these studies, it became widely accepted that rational selection was superior to a random selection. As the rational selection and appropriate molecular characterization were needed, informative descriptors have been increasingly developed.[3,4] In order to produce a mathematical description for the molecules of interest, we applied 3D descriptors[5,6] to a subset chosen by a 2D fingerprint. In this work, we follow this line of thought and apply these approaches to the discovery processes of Cannabinoid-1 (CB1) antagonists. The CB1 receptor belongs to the rhodopsin (Rho) subfamily of G protein-coupled receptors (GPCRs), which approximately 30% of clinically marketed drugs.[7] The CB1 receptor antagonists/inverse agonists represent a promising new approach for reducing body weight and decreasing the co-morbidities associated with excessive adiposity.[8] To formulate a predictive model for CB1 antagonists, we used the ligand- and structure-based modeling tools. For structure-based modeling approaches, we built a homology model based on the X-ray structure of rhodopsin because of the absence of a reliable CB1 crystal structure. We also selected diverse compounds using a maximum dissimilarity method with 2D-fingerprints and then clustered diverse compounds into subset in order to select a representative structure in training and test set. We built the predictive models via modified pharmacophore, 3D-QSAR,

and interaction field methods and indirectly suggested the CB1 putative active site model.

We collected 187 CB1 antagonists,[9–16] and filtered antagonists through MDDR and CMC criteria[17,18] to remove non-druglike compounds, finally leading to a selection of 53 compounds. After these compounds were converted using CONCORD,[19] they were minimized using Gasteiger–Hückel charges and conjugated gradient methods. In order to consider structural redundancy and the range of biological activity of the subset, we carried out the maximum dissimilarity study using the Extended Connectivity Fingerprints (ECFP).[4] We selected 36 compounds as the training set and 17 compounds as the test set. This represents a spread of over four orders of biological activity. We classified 36 compounds in the training set into eight clusters and selected eight representative structures from each cluster based on measures of good activity and distance from the center of each cluster. The structures of these compounds are shown in Table 1. We used taranabant[14] and rimonabant[15] and as templates. Compounds in Table 1 were docked into the CB1 homology model based on the used templates in order to set reasonable binding conformation. We obtained a good model having high correlation between the energy score (D_Score) and CB1 antagonist activities ($R^2 = 0.58$).
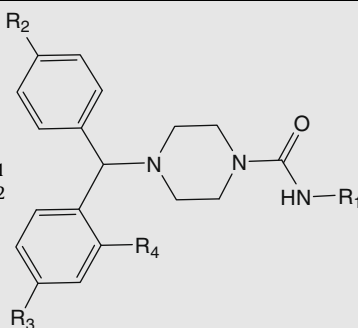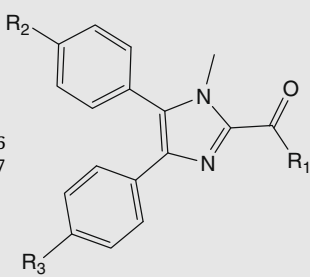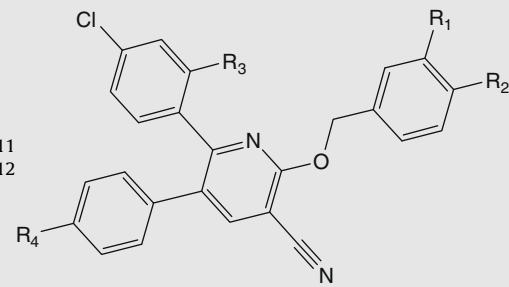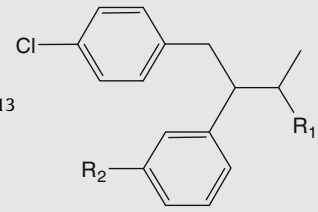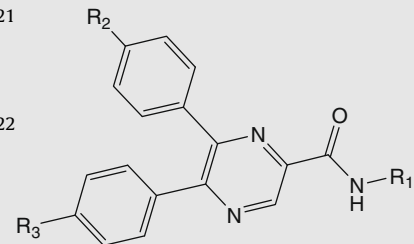
Common feature pharmacophores are generated using the Hip-HopRefine algorithm.[20] HipHopRefine was configured to allow for a maximum of 100 excluded volumes to be added to the generated pharmacophore hypotheses. It then identifies the 3D spatial arrangement of chemical features of real active compounds and removes false positives in virtual screening. Hypotheses parameters employed were *Principal* and *MaxOmitFeat*. Accordingly, $pIC_{50}$ values >8, $pIC_{50}$ values between 6 and 7, and $pIC_{50}$ values <5 were regarded as active, moderate, and inactive compounds, respectively;

* Corresponding author.
*E-mail address:* nskang@krict.re.kr (N.S. Kang).

**Table 1**
The compounds in the training set

| Number | pIC$_{50}$ | R$^1$ | R$^2$ | R$^3$ | R$^4$ |
|---|---|---|---|---|---|



| Number | pIC$_{50}$ | R$^1$ | R$^2$ | R$^3$ | R$^4$ |
|---|---|---|---|---|---|
| 1 | 6.40 | CH(CH$_3$)$_3$ | Cl | H | Cl |
| 2 | 6.11 | CH(CH$_3$)$_3$ | Br | H | Cl |
| 3 | 5.66 | CH(CH$_3$)$_3$ | Cl | H | CH$_3$ |
| 4 | 5.46 | Methylcyclobutane | Cl | Cl | H |
| 5 | 5.18 | CH(CH$_3$)$_3$ | Cl | H | CF$_3$ |



| Number | pIC$_{50}$ | R$^1$ | R$^2$ | R$^3$ | R$^4$ |
|---|---|---|---|---|---|
| 6 | 6.33 | Piperidin-1-amine | CH$_3$ | CH$_3$ | |
| 7 | 5.72 | Piperidin-1-amine | H | H | |
| 8 | 5.74 | Cyclohexanamine | H | H | |
| 9 | 5.46 | Piperidine | CH$_3$ | CH$_3$ | |
| 10 | 4.72 | Piperidine | H | H | |



| Number | pIC$_{50}$ | R$^1$ | R$^2$ | R$^3$ | R$^4$ |
|---|---|---|---|---|---|
| 11 | 8.20 | F | F | Cl | CH$_3$ |
| 12 | 5.55 | H | H | H | H |



| Number | pIC$_{50}$ | R$^1$ | R$^2$ | R$^3$ | R$^4$ |
|---|---|---|---|---|---|
| 13 | 9.52 | 2-Methyl-2-(5-(trifluoromethyl)pyridin-2-yloxy)propanamide | CN | | |
| 14 | 8.95 | 2-(3,5-Difluorophenoxy)-2-methylpropanamide | H | | |
| 15 | 8.88 | 2-(5-Chloropyridin-2-yloxy)-2-methylpropanamide | H | | |
| 16 | 8.82 | 2-(3-Chlorophenoxy)-2-methylpropanamide | H | | |
| 17 | 7.77 | 2-Methyl-2-(pyridin-4-yloxy)propanamide | H | | |
| 18 | 7.68 | Phenylmethanesulfonamide | CN | | |
| 19 | 5.77 | 2-Methylpropane-2-sulfonamide | CN | | |
| 20 | 5.69 | Methanesulfonamide | CN | | |
| 21 | 5.69 | Methanesulfonamide | CN | | |



| Number | pIC$_{50}$ | R$^1$ | R$^2$ | R$^3$ | R$^4$ |
|---|---|---|---|---|---|
| 22 | 7.79 | Cyclohexane | OCH$_3$ | OCH$_3$ | |

**Table 1** (*continued*)

| Number | pIC$_{50}$ | R$^1$ | R$^2$ | R$^3$ | R$^4$ |
|--------|------------|-------|-------|-------|-------|
| 23 | 6.62 | Phenyl | OCH$_3$ | OCH$_3$ | |
| 24 | 5.25 | Phenyl | H | H | |
| 25 | 8.21 | N | N | C(CH$_3$) | Cl |
| 26 | 5.65 | C | O | N | H |
| 27 | 5.22 | C | NH | N | H |
| 28 | 8.09 | Cl | H | Cl | H |
| 29 | 7.92 | CH$_3$ | H | CH3 | H |
| 30 | 7.37 | OCH$_3$ | H | OCH$_3$ | H |
| 31 | 6.45 | H | Cl | H | Cl |
| 32 | 5.81 | H | H | H | H |
| 33 | 7.45 | CN | | | |
| 34 | 6.95 | H | | | |
| 35 | 6.77 | | | | |
| 36 | 8.72 | | | | |

**Table 2**
Hypotheses results; 211 compounds were used including 49 active compounds and 162 inactive compounds

| Hypotheses | Features | Number of excluded volumes | Active (49)/ inactive (162)[a] |
|---|---|---|---|
| 1 | Hba 1, Hy 4, Hya 1 | 100 | 36.7/6.2[b] |
| 2 | Hba 1, Hy 2, Hya 2 | 100 | 57.12/3.1 |
| 3 | Hba 1, Hy 4, Hya 1 | 100 | 49.0/8.6 |
| 4 | Hba 1, Hy 2, Hya 1, Ra 1 | 100 | 57.1/3.1 |
| 5 | Hba 1, Hy 2, Hya 1, Ra 1 | 100 | 55.1/12.3 |
| 6 | Hba 1, Hy 2, Hya 1, Ra 1 | 100 | 67.3/3.7 |
| 7 | Hba 1, Hy 2, Hya 1, Ra 1 | 100 | 61.2/3.7 |
| 8 | Hba 1, Hy 2, Hya 1, Ra 1 | 100 | 65.3/7.4 |
| 9 | Hba 1, Hy 2, Hya 2 | 100 | 59.2/3.1 |
| 10 | Hba 1, Hy 2, Hya 2 | 100 | 61.2/6.8 |

[a] The total number of used compounds.
[b] The percentage (%) of well mapped compounds.

they were assigned appropriate values for Principal and MaxOmit-Feat parameters. The predefined pharmacophore features are used to automatically create the pharmacophores hypothesis model. The list of features of minimum and maximum values were as follows: H-bond acceptor (Hba) 1 and 5, H-bond donor (Hbd) 0 and 5, Hydrophobic (Hy) 2 and 5, Hydrophobic aromatic (Hya) 1 and 5, and Ring aromatic (Ra) 0 and 5.

We used two alignments on the same training set compounds to carry out CoMFA[21] and CoMSIA[22] calculation: one is based on a receptor-aligned model from the docking pose and the other is based on a pharmacophore-aligned model from the HipHopRefine generation. We performed a Partial Least Square (PLS) statistical analyses in order to obtain the linear correlation coefficients between the experimental and calculated activities using the Leave-One-Out cross-validation with the condition of 2.0 kcal/mol column filtering.
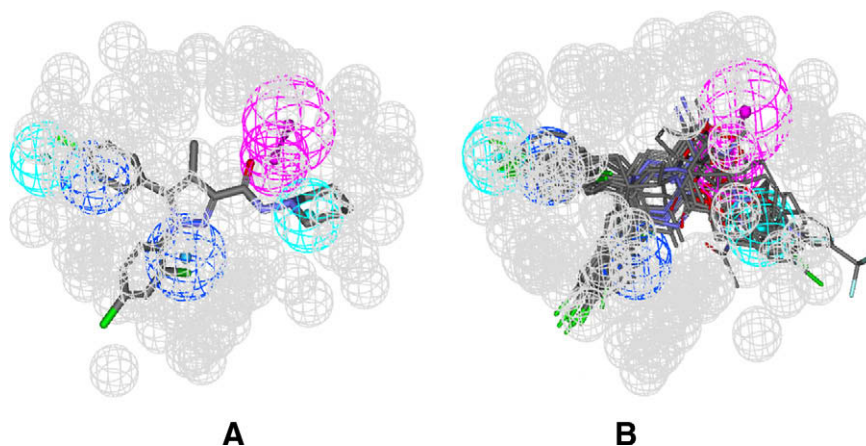


**Figure 1.** The pharmacophore features of HipHopRefine, H-bond acceptor, Hydrophobics and Hydrophobic aromatics show in magenta, cyan and blue. Gray spheres represent the excluded volumes; (A) is the pharmacophore mapping for rimonabant and (B) for test set compounds.
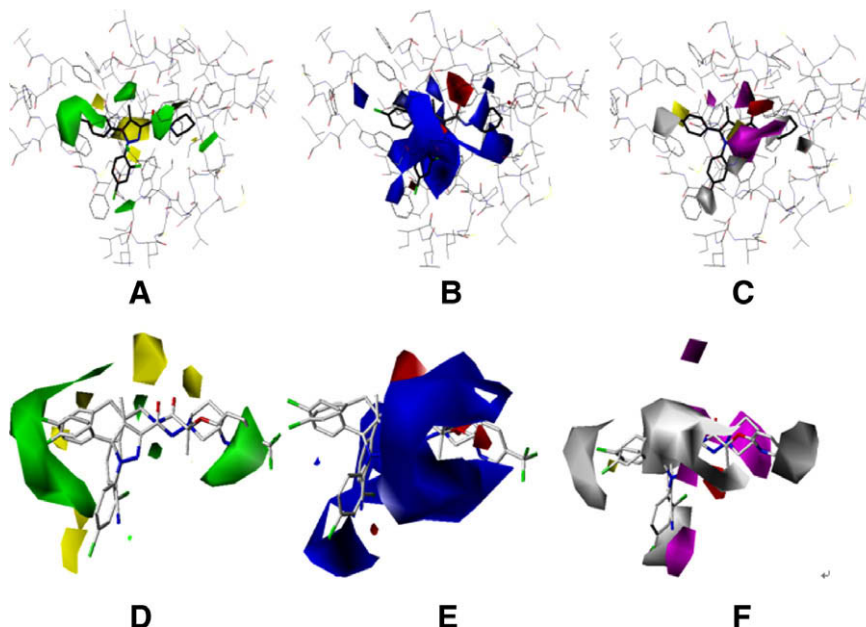


**Figure 2.** CoMFA and CoMSIA contour maps. A, B and C contour maps indicate receptor-based alignment CoMFA and CoMSIA. D, E and F indicate pharmacophore-based alignment CoMFA and CoMSIA. In the CoMFA contour maps, favorable areas for steric and electrostatic appeared in green and blue, and disfavorable area in yellow and red, respectively. In the CoMSIA maps, for steric and electrostatic were the same as CoMFA maps and favorable area for H-bonding acceptor and hydrophobic appeared in magenta and white, unfavorable area in red and yellow, respectively.

**Table 3**
CoMFA and CoMSIA PLS results

| PLS statistics | Receptor-based | | Pharmacohpore-based | |
| --- | --- | --- | --- | --- |
| | CoMFA | CoMSIA | CoMFA | CoMSIA |
| $q^2$ | 0.57 | 0.51 | 0.51 | 0.47 |
| $r^2$ | 0.97 | 0.97 | 0.98 | 0.97 |
| Standard deviation | 0.23 | 0.26 | 0.18 | 0.22 |
| PLS components | 5 | 5 | 5 | 5 |
| Field contribution | | | | |
| Steric:electrostatic | 0.53:0.46 | 0.11:0.41 | 0.53:046 | 0.14:0.25 |
| hydrophobic | | 0.27 | | 0.34 |
| H-Bond acceptor | | 0.20 | | 0.25 |

**Table 4**
Experimental versus predictive $pIC_{50}$ for the test set obtained from receptor-based alignment

| Number | $pIC_{50}$[a] | CoMFA | | CoMSIA | |
| --- | --- | --- | --- | --- | --- |
| | | $pIC_{50}$ | Residual[b] | $pIC_{50}$ | Residual |
| 37 | 7.74 | 7.09 | −0.65 | 7.66 | −0.07 |
| 38 | 8.09 | 7.50 | −0.58 | 7.99 | −0.1 |
| 39 | 8.14 | 7.27 | −0.86 | 8.37 | 0.22 |
| 40 | 7.18 | 6.74 | −0.44 | 7.12 | −0.05 |
| 41 | 7.77 | 6.8 | −0.97 | 7.64 | −0.12 |
| 42 | 7.67 | 6.96 | −0.71 | 7.47 | −0.20 |
| 43 | 7.74 | 7.02 | −0.72 | 7.09 | −0.65 |
| 44 | 7.58 | 6.93 | −0.65 | 6.69 | −0.88 |
| 45 | 8.52 | 8.91 | 0.39 | 8.66 | 0.14 |
| 46 | 7.69 | 7.93 | 0.23 | 7.61 | −0.08 |
| 47 | 7.74 | 8.41 | 0.66 | 7.84 | 0.09 |
| 48 | 8.69 | 8.03 | −0.66 | 8.34 | −0.35 |
| 49 | 8.79 | 8.57 | −0.22 | 8.88 | 0.08 |
| 50 | 8.74 | 8.52 | −0.22 | 8.74 | −0.00 |
| 51 | 9.30 | 8.52 | −0.77 | 8.69 | −0.60 |
| 52 | 6.13 | 6.39 | 0.25 | 6.69 | 0.55 |
| 53 | 7.49 | | | 7.49 | 0.00 |

[a] Experimental $pIC_{50}$
[b] Residual = predicted $pIC_{50}$ – experimental $pIC_{50}$.

As the other prediction model, we performed Molecular Interaction Fields (MIFs)[23] calculations which allow us the independent alignment of molecules. MIFs calculate chemical probes that represent important interactions for ligand binding at the active site of target, and thus identify regions where favorable virtual chemical groups could interact and decide 3D surfaces where an interaction with groups of a potential receptor would occur favorably. GRid INdependent Descriptors (GRIND)[24] transforms the information included in the MIFs and generates from them a handful of informative variables independent of the location of the molecules within

**Table 5**
Predicted $pIC_{50}$ values from GRIND descriptors for the training and test set

| Number | $pIC_{50}$ | Number | $pIC_{50}$ | Number | $pIC_{50}$ |
| --- | --- | --- | --- | --- | --- |
| 1 | 5.99 | 19 | 6.03 | 37 | 7.85 |
| 2 | 6.10 | 20 | 5.91 | 38 | 8.13 |
| 3 | 5.72 | 21 | 5.09 | 39 | 8.03 |
| 4 | 5.54 | 22 | 7.19 | 40 | 7.30 |
| 5 | 5.13 | 23 | 7.13 | 41 | 7.77 |
| 6 | 6.44 | 24 | 5.83 | 42 | 7.81 |
| 7 | 5.72 | 25 | 7.91 | 43 | 7.58 |
| 8 | 6.10 | 26 | 5.65 | 44 | 7.55 |
| 9 | 5.38 | 27 | 5.66 | 45 | 8.70 |
| 10 | 4.66 | 28 | 7.51 | 46 | 7.55 |
| 11 | 8.44 | 29 | 6.63 | 47 | 8.02 |
| 12 | 5.91 | 30 | 7.30 | 48 | 8.32 |
| 13 | 9.42 | 31 | 6.64 | 49 | 8.80 |
| 14 | 8.87 | 32 | 5.88 | 50 | 8.56 |
| 15 | 8.83 | 33 | 7.41 | 51 | 9.42 |
| 16 | 8.94 | 34 | 7.03 | 52 | 6.20 |
| 17 | 7.63 | 35 | 7.22 | | |
| 18 | 7.87 | 36 | 9.08 | | |

the grid. To generate a CB1 molecular interaction field on the same training set, we use probes representing strong non-covalent interactions commonly found in the receptors: hydrophobic (Dry), hydrogen bond acceptor (O), hydrogen bond donor (N1). GRIND were generated, analyzed, and interpreted using the ALMOND[25] program.

As shown in Table 2 and Figure 1, the HipHopRefine pharmacophore results were consistent with previous findings.[26,27] As shown in Figure 1A, carbonyl oxygen of rimonabant interacted with K192 side chain (NZ), producing key interaction of CB1 antagonists and forming salt bridge with D366, and with three hydrophobic sites including aromatic features located near F200/W279/W356, W255/Y275/F278, V196/F170/M385/L387/on Helix 5, 6, 7. F200/W279/W356 residues interacted with the 2,4-dichlorophenyl ring of rimonabant, W255/Y275/F278 residues interacted with 4-chlorophenyl ring of rimonabant, and V196/F170/M385/L387/residues formed large hydrophobic cavities where piperidinyl groups of rimonabant could fit comfortably. Figure 1B shows how compounds in the test set fit in our pharmacophore model. Generated hypotheses agree with the common 3D configurations of CB1 functional features.

The CoMSIA contour maps, for steric and electrostatic interaction, were the same as CoMFA contour maps as shown in Figure 2. The red CoMFA contour around the carbonyl group (electronegative) matched well with the highly electropositive K192 side chain of the active site in Figure 2B. The overall large blue CoMFA
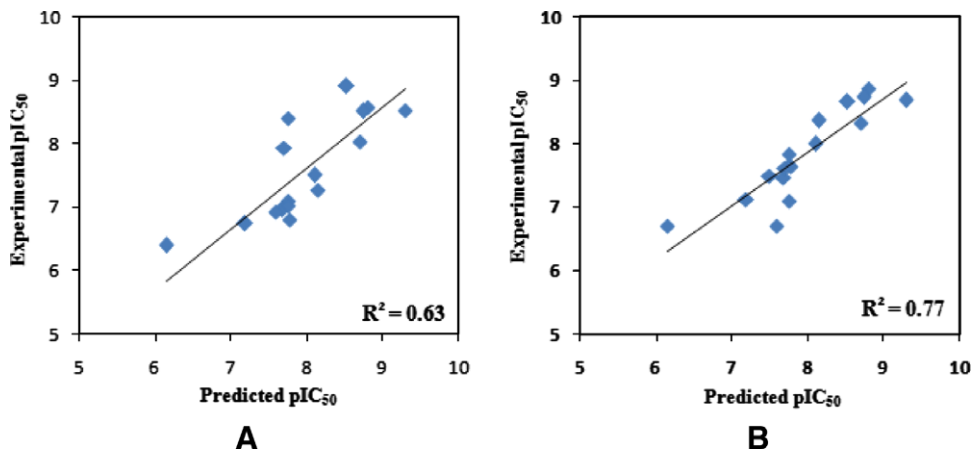


**Figure 3.** Correlation plots between experimental and predictive activity from receptor-based alignment obtained from CoMFA (A) and CoMSIA (B) results for the test set.
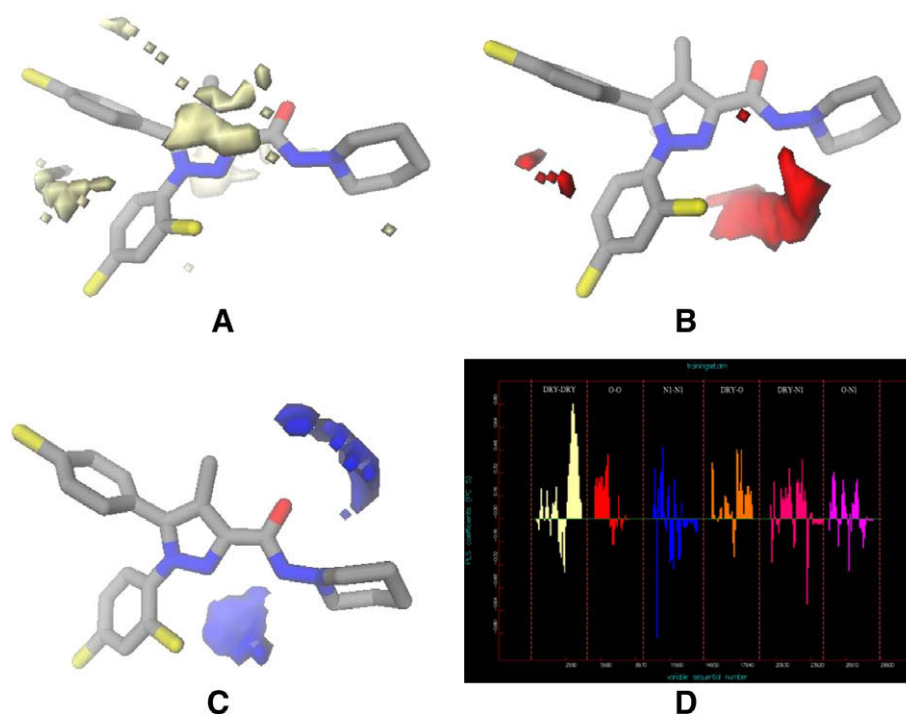
**Figure 4.** Favorable interaction fields with each probe. A, B and C indicate hydrophobic (Dry), H-bond acceptor (O) and H-bond donor (N1) probes. D is PLS coefficient profile. Each peak indicates an interaction field. Dry–Dry, O–O and N1–N1 interaction were shown in ivory, red and blue and Dry–O, DRY–N1 and O–N1 interaction in orange, pink and violet.

contour map also is complementary to the electron-rich group effect, such as π-stacking interactions with F200/W279/W356, W255/Y275/F278 and V196/F170/ M384/L387 in the active site. In the steric interaction, both ends are represented by green, which indicates that bulky hydrophobic groups of both sides improved activity. As it is shown in Table 1, halogen atoms and $CF_3$ are sufficient to enhance activity, and they correspond with the contour maps.

The CoMSIA maps are similar to the CoMFA maps, especially the large white and magenta maps, which indicate necessary hydrophobic and hydrogen acceptor interactions with the active site residues. Both the CoMFA and CoMSIA contour maps from receptor-based and pharmacophore-based alignments are consistent with the pharmacophore model as key interaction points. However, receptor-based alignment of CoMFA and CoMSIA afforded better PLS analyses and predictive values for the test set than the pharmacophore-based alignment. CoMFA and CoMSIA PLS according to alignment methods were shown in Tables 3 and 4 and Figure 3.

The Almond program gives graphical as well as statistical results. In particular, analysis of the PLS coefficients profiles indicates the most significant GRIND variables for a given model, which are positive and negative values correlated to biological activity. Predicted $pIC_{50}$ and the PLS coefficient profile for CB1 activity are shown in Table 5 and Figure 4.

Each peak in the PLS coefficient profile indicates an interaction field. Dry–Dry, O–O and N1–N1 interaction in the autocorrelograms (the same MIF) were shown in ivory, red and blue and Dry–O, Dry–N1 and O–N1 interaction in the cross-correlograms (the different MIF) were shown in orange, pink and violet. Auto and cross-correlograms are generated based on the MIFs using a maximum auto and cross-correlograms (MACC) algorithm.[28]

The height of the peak expresses the product of the intensity of the field on both nodes that are separated by a distance corresponding to the abscissa of the profile. Short distances of node-node interaction appear on the left side and longer distances on the right side. The shape of the peak is also relevant: wide peaks tend to represent intense interactions; narrow peaks tend to represent weaker interactions. Overall, Dry and N1 correlograms expresses intensive and wide peaks, which reflect interactions with aromatic side chains and hydrogen bonding with K192 of the active site. These are therefore recognized by the model as important structural features in the CB1 homology active site. Both the CB1 PLS coefficient profile and the graphical result for rimonabant correspond to the pharmacophore and 3D-QSAR results as previously mentioned. The statistical results gives Leave-one-out cross-validation of $q^2 = 0.46$ with five components and no validation $r^2 = 0.92$ with a standard deviation of 0.38. Validation for the test set is better than the 3D-QSAR models.

In this study, we examined the effect of the prediction model by reasonable classification. We built two prediction models via 3D-QSAR including CoMFA and CoMSIA, and a MIFs model. Result obtained from each model provides important data for high throughput virtual screening and also can suggest the putative binding model for CB1 antagonists.

### Acknowledgement

### References and notes

1. Pötter, T.; Matter, H. *J. Med. Chem.* **1998**, *41*, 478.
2. Patterson, D. E.; Cramer, R. D.; Ferguson, A. M.; Clark, R. D.; Weinberger, L. E. *J. Med. Chem.* **1996**, *39*, 3049.
3. Matter, H. *J. Med. Chem.* **1997**, *40*, 1219.
4. Hert, J.; Willett, P.; Wilton, D. J.; Acklin, P.; Azzaoui, K.; Jacoby, E.; Schuffenhauer, A. *J. Chem. Inf. Comput. Sci.* **2004**, *44*, 1177.
5. Cruciani, G. Molecular Interaction Fields. In *Methods and Principles in Medicinal Chemistry*; Manhold, R., Kubinyi, H., Folkers, G., Eds.; Wiley-VCH, 2006; Vol. 27,.
6. Sciabola, S.; Carosati, E.; Sanchez, L. C.; Baroni, M.; Mannhold, R. *Bioorg. Med. Chem.* **2007**, *15*, 6450.
7. Wise, A.; Gearing, K.; Rees, S. *Drug Discovery Today* **2002**, *7*, 235.

8. Pi-Sunyer, F. X.; Aronne, L. J.; Heshmati, H. M.; Devin, J.; Rosenstock, J. *J. Am. Med. Assoc.* **2006**, *295*, 761.
9. Boström, J.; Berggren, K.; Elebring, T.; Greasley, P. J.; Wilstermann, M. *Bioorg. Med. Chem.* **2007**, *15*, 4077.
10. Meurer, L. C.; Finke, P. E.; Mills, S. G.; Walsh, T. F.; Toupence, R. B.; Goulet, M. T.; Wang, J.; Tong, X.; Fong, T. M.; Lao, J.; Schaeffer, M. T.; Chen, J.; Shen, C. P.; Stribling, D. S.; Shearman, L. P.; Strack, A. M.; Van der Ploeg, L. H. T. *Bioorg. Med. Chem. Lett.* **2005**, *15*, 645.
11. Plummer, C. W.; Finke, P. E.; Mills, S. G.; Wang, J.; Tong, X.; Doss, G. A.; Fong, T. M.; Lao, J. Z.; Schaeffer, M. T.; Chen, J.; Shen, C. P.; Stribling, D. S.; Shearman, L. P.; Strack, A. M.; Van der Ploeg, L. H. T. *Bioorg. Med. Chem. Lett.* **2005**, *15*, 1441.
12. Song, K. S.; Lee, S. H.; Chun, H. J.; Kim, J. Y.; Jung, M. E.; Ahn, K. W.; Kim, S. U.; Kim, J. M.; Lee, J. H. *Bioorg. Med. Chem.* **2008**, *16*, 4035.
13. Debenham, J. S.; Madsen-Duggan, C. B.; Walsh, T. F.; Wang, J.; Tong, X.; Doss, G. A.; Lao, J.; Fong, T. M.; Schaeffer, M. T.; Xiao, J. C.; Huang, C. R.; Shen, C. P.; Fang, Y.; Marsh, D. J.; Stribling, D. S.; Shearman, L. P.; Strack, A. M.; MacIntyre, D. E.; Van der Ploeg, L. H. T.; Goulet, M. T. *Bioorg. Med. Chem. Lett.* **2006**, *16*, 681.
14. Lin, L. S.; Lanza, T. J.; Jewell, J. P.; Liu, P.; Shah, S. K.; Qi, H.; Tong, X.; Wang, J.; Xu, S. S.; Fong, T. M.; Shen, C. P.; Lao, J.; Xiao, J. C.; Shearman, L. P.; Stribling, D. S.; Rosko, K.; Strack, A.; Marsh, D. J.; Feug, Y.; Kumar, S.; Samuel, K.; Yin, W.; Van der Ploeg, L. H. T.; Goulet, M. T.; Hagmann, W. K. *J. Med. Chem.* **2006**, *49*, 7584.
15. Armstrong, H. E.; Galka, A.; Lin, L. S.; Lanza, T. J.; Jewell, J. P.; Shah, S. K.; Guthinkonda, R.; Truong, Q.; Chang, L. L.; Quaker, G.; Colandrea, U. J.; Tong, X.; Wang, J.; Xu, S.; Fong, T. M.; Shen, C. P.; Lao, J.; Chen, J.; Shearman, J. P.; Stribling, D. S.; Rosko, K.; Strack, A.; Ha, S.; Van der Ploeg, L. H. T.; Goulet, M. T.; Hagmann, W. K. *Bioorg. Med. Chem. Lett.* **2007**, *17*, 2184.
16. Lange, J. H. M.; van Stuivenberg, H. H.; Veerman, W.; Wals, H. C.; Stork, B.; Coolen, H. K. A. C.; McCreary, A. C.; Tiny, J. P.; Kruse, A. C. G. *Bioorg. Med. Chem. Lett.* **2005**, *15*, 4794.
17. Ghose, A. K.; Viswanadhan, V. N.; Wendoloski, J. J. *J. Comb. Chem.* **1999**, *1*, 55.
18. Oprea, T. I. *J. Comput. Aided Mol. Des.* **2000**, *14*, 251.
19. CONCORD; Tripos Inc., 1699 South Hanley Road, St. Louis, MO 63144.
20. Taha, M. O.; Bustanji, Y.; Al-Bakri, A. G.; Yousef, A. M.; Zalloum, W. A.; Al-Masri, I. M.; Atallah, N. *J. Mol. Graphics Modell.* **2007**, *25*, 870.
21. Cramer, R. D.; Patterson, D. E.; Bunce, J. D. *J. Am. Chem. Soc.* **1988**, *110*, 5959.
22. Klebe, G.; Abraham, U. *J. Comput. Aided Mol. Des.* **1999**, *13*, 1.
23. Goodford, P. J. *J. Med. Chem.* **1985**, *28*, 849.
24. Pastor, M.; Cruciani, G.; McLay, I.; Pickett, S.; Clementi, S. *J. Med. Chem.* **2000**, *43*, 3233.
25. Molecular Discovery Ltd., http://www.moldiscovery.com.
26. Hurst, D. P.; Lynch, D. L.; Barnett-Norris, J.; Hyatt, S. M.; Seltzman, H. H.; Zhong, M.; Song, Z. H.; Nie, J.; Lewis, D.; Reggio, P. H. *Mol. Pharmacol.* **2002**, *62*, 1274.
27. Murphy, J. W.; Kendall, D. A. *Biochem. Pharmacol.* **2003**, *65*, 1623.
28. Broto, P.; Moreau, G. *Eur. J. Med. Chem.* **1984**, *19*, 66.